AIAA AVIATION Forum
5-9 June 2017, Denver, Colorado
35th AIAA Applied Aerodynamics Conference

10.2514/6.2017-3054

Trim Routine for Multirotor Vehicles in Straight and Level Flight

Tsaltas, Julia D.[1] and Bramesfeld, Götz[2]
Ryerson University, Toronto, Ontario, Canada, M5B2K3

This paper introduces a flight performance prediction method for multirotor vehicles. Besides trimming for forces during and estimating power required, the method also computes the residual moments. The chosen approach uses a force and moment decomposition approach that estimates the aerodynamic loads of the individual elements of a given vehicle configuration and flight condition. By evaluating the aerodynamic forces and moments of a vehicle using first principles of aerodynamics, stability and control models can be better predicted during the design phase of a new multirotor vehicle or when expanding the flight envelope of an existing vehicle. In this paper, the residual moments of the multirotor vehicle in steady, straight and level flight are calculated for the flight envelope using a trim routine. The rotor data is based on prediction or experimental data. Initial comparisons with flight test data show agreement. Ultimately, the method supports the development of unmanned multirotor vehicle control laws.

Nomenclature

α	=	angle of attack
α_R	=	effective inflow angle of attack
α_{int}	=	change in inflow angle due to mutual rotor interference
θ	=	pitch angle
D_{par}	=	parasitic drag
$D_{ind,body}$	=	induced drag of the body
L_{body}	=	lift of the body
M_x	=	rotor rolling moment
M_y	=	rotor pitching moment
RPM	=	rotor speed in revolutions per minute
P_{rot}	=	rotor power
P_{ind}	=	induced power
P_{int}	=	interference power due to mutual rotor interference
P_{par}	=	total parasitic power of the fuselage
P_{pro}	=	rotor profile power
P_{tot}	=	total rotor power
P_x	=	normal rotor force
P_y	=	side rotor force
T	=	thrust
V_∞	=	freestream velocity
$v_{int,z}$	=	mutual interference velocity through rotor plane
V_R	=	effective inflow velocity
W	=	vehicle weight
x_H, y_H, z_H	=	horizontal reference frame
x_R, y_R, z_R	=	rotor reference frame

[1] Graduate Student, Department of Aerospace Engineering, Ryerson University, Student Member AIAA
[2] Assistant Professor, Department of Aerospace Engineering, Ryerson University, Member AIAA

I. Introduction

THE development of control systems for multirotor vehicles traditionally relies on relatively simplistic aerodynamic models for the prediction of their flight dynamics. Rather than using more comprehensive aerodynamics models, reliable control laws are often developed using extensive flight testing, which is relatively resource intense. Examples of simplistic aerodynamic models include simple quadratic relationships between thrust and rotor-rotational speeds that neglect effects such as advance ratio, inflow conditions, and the impact of the other rotors and fuselage whose presence alter the local flow field due to their close proximity. All of these results lead to highly nonlinear responses of multirotor vehicles that are difficult to fully capture using the relatively simplistic approaches that are often used.

Recent control systems research for multirotor vehicles uses more complex aerodynamic models for the rotors, for example Refs. 1, 2 and 3. Nevertheless, most multirotor performance prediction methods still lack the ability to fully capture the complex aerodynamics that result from the interaction of several rotors that operate in close proximity and the impact of different shapes of payloads. For example, Ref. 4 models with limited success the mutual interaction of several rotors using a fixed-wing wake analogy. Hoffmann et al. focused on improving the dynamic model.[5] In their previous research they had determined that the precision of trajectory control was directly dependent on the quality of the aerodynamic models that are used.[6] This was found to be particularly true with increasing flight speed. Similarly, Powers et al. conducted a series of flight tests near obstacles. In these tests, the control gains for motor control were corrected based on positioning errors.[7] The authors identified that the main control model of a multirotor vehicle is a complex function of motor speeds and environmental conditions. Overall, the complex aerodynamics related to multirotor vehicles make their reliable control a technical challenge.

This paper presents a multirotor vehicle flight performance prediction model. The model considers the impact of the fuselage, the interaction of several thrusting rotors that are in close proximity to each other, as well as the effect related to trims. For each rotor, the method finds the rotational speeds and powers that are required for steady and level flight. The required rotor loads are determined using a table lookup routine based on the rotor-inflow conditions. Although the method does not fully trim the vehicle, the residual moments are estimated, that is, the moments that remain after the force-trim routine for a particular flight and vehicle configuration. This allows the assessment of the moment changes of various flight configurations. The multirotor vehicle performance model is an expansion of the model presented in Ref. 8. Overall, the method is computationally fast and allows to gain insight about the aerodynamics and stability needs of multirotor vehicles.

II. Multirotor Vehicle Model

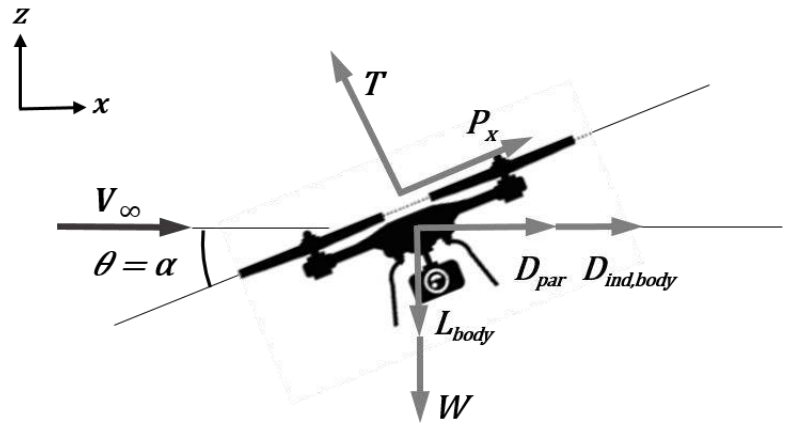

Figure 1: Free-body diagram of aerodynamic forces on a multirotor vehicle

A. Equations of Motion for Longitudinal Force Trim

Figure 1 shows a free-body diagram of the major forces that act in the longitudinal plane of a multirotor vehicle. During steady and level flight, the loads that the rotor develops, trust T and normal force P_x, must be in equilibrium with the vehicle weight, W, and the aerodynamic forces of the fuselage, namely drag, D_{par} and D_{ind}, and negative lift, L_{body}. The equations of motion are based on the set that was developed for the multirotor vehicle performance model Ref. 8 and expanded to include forces on the body related to its lift. Only longitudinal forces, such as thrust, normal

force, drag, body lift, and weight are considered for force trim. Lateral forces, P_y, used in the trim routine or crosswind effects are not considered in the scope of this paper.

The horizontal and vertical force equilibrium equations of the vehicle are:

$$0 = D_{par} + D_{ind,body} + P_x \cos\theta - T \sin\theta \quad \text{(Eq. 1)}$$

and

$$0 = T \cos\theta + P_x \sin\theta - L_{body} - W \quad \text{(Eq. 2)}$$

Rearranging Eq. 2 for $\cos\theta$:

$$\cos\theta = \frac{W + L_{body} - P_x \sin\theta}{T} \quad \text{(Eq. 3)}$$

Substituting Eq. 3 into Eq. 1 and multiplying all terms by thrust, T, yields:

$$0 = TD_{par} + TD_{ind,body} + P_x(W + L_{body} - P_x \sin\theta) - T^2 \sin\theta \quad \text{(Eq. 4)}$$

Rearranging for $\sin\theta$ gives an expression for pitch angle required for force trim:

$$\sin\theta = \frac{P_x W + P_x L_{body} + TD_{par} + TD_{ind,body}}{T^2 + {P_x}^2} \quad \text{(Eq. 5)}$$

Substituting pitch angle, θ, into Eq. 3 yields thrust:

$$T = \frac{W + L_{body} - P_x \sin\theta}{\cos\theta} \quad \text{(Eq. 6)}$$

Thrust is evenly distributed between the number of rotors. Based on this thrust and the inflow conditions, the rotational speed is determined for each rotor using tabulated rotor-performance data. The tabulated data also contains power required and the remaining thrust loads that the rotor develops under those conditions, for example the normal force, P_x. The tabulated rotor performance data is based on either experimental or prediction data. Based on the rotor conditions, the interaction between the rotors is determined and used to update Eqs. 5 and 6.

B. Rotor Loads

The loads developed of a rotor greatly depend on its rotational speed and inflow conditions as it is shown in Fig. 2, which shows the predicted and measured thrust coefficients of a single small rotor. Using similar data as presented in this figure, and the thrust required that is determined using Eq. 6, the required rotational speed can be determined. Once the rotational speed is determined, the remaining rotor conditions are determined. These conditions include power required, any moments as well as the normal forces that the rotor develops.

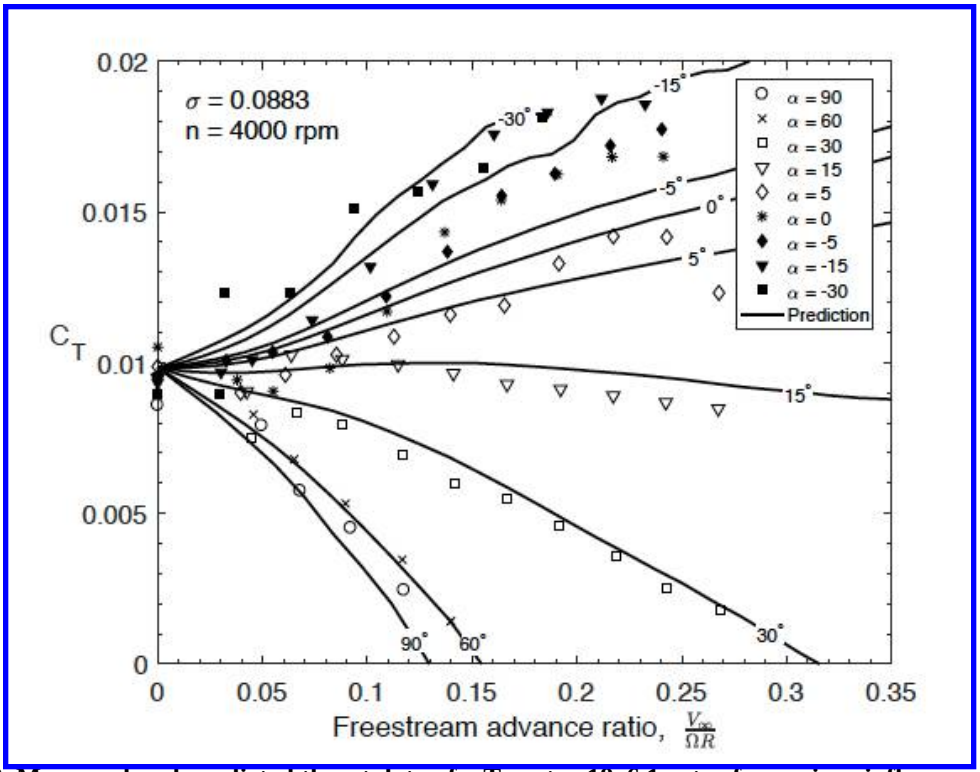

Figure 2. Measured and predicted thrust data of a T-motor 18x6.1 rotor for various inflow conditions.[9]

Unlike for the single rotor conditions that are presented in Figure 2, in the case of a multirotor vehicle the inflow conditions of each rotor may differ depending on the particular rotor and flight condition. Due to the close proximity of the rotors the flow fields of each rotor are modified compared to the freestream conditions. These additional inflow component, which is referred to as mutual interference velocity, changes significantly for each rotor depending its location relative to the other rotors and the flight conditions. For example, during forward flight, the wakes coming of the lead rotors have great impacts on the rear rotors than the other way around. The mutual interference greatly affects the performance of the individual rotors of the formation.

In the herein presented approach, the mutual rotor interference is modelled using a series of vortex rings that represent the wake coming of each rotor[8]. The model is a discretized representation of the analytical result of a vortex tube [10]. For each rotor, the orientation of this discretized vortex tube wake is determined using the freestream inflow conditions and a momentum-theory based induced velocity. Based on each wake shape, the perturbation velocities are determined at the other rotor discs.

For each individual rotor, the effective inflow angle changes due to the perturbation velocity, v_{int}, that is due to the influence of the other rotors. Based on the velocities in Fig. 3, the effective inflow velocity and angle of attack are:

$$\bar{V}_R = \sqrt{(V_\infty - v_{int,z}\sin\theta)^2 + (v_{int,z}\cos\theta)^2} \quad \text{(Eq. 7)}$$

$$\bar{\alpha}_R = \theta - \alpha_{int} \quad \text{(Eq. 8)}$$

where V_∞ is the freestream velocity, $v_{int,z}$, is the mutual interference velocity in perpendicular to the rotor plane, and α is the freestream flow angle. α_{int} is the change in inflow angle due to the influence of $v_{int,z}$.

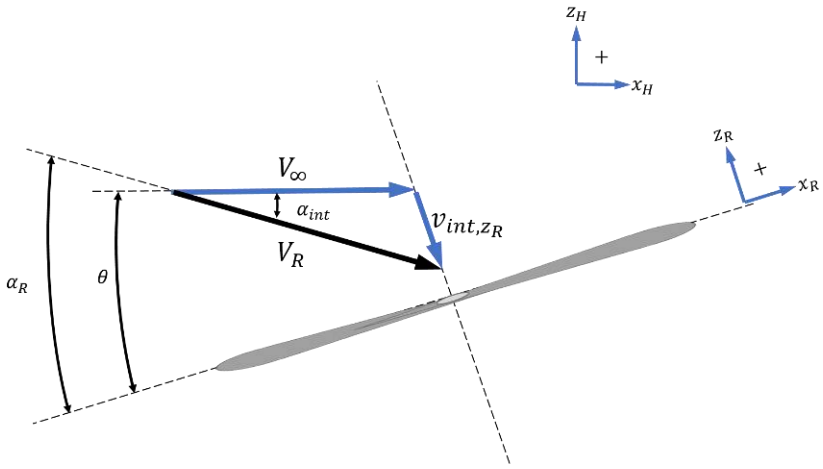

Figure 3: Mutual interference velocity applied to a rotor resulting in an increased inflow velocity and inflow angle relative to freestream velocity and angle

It must be noted that as the rotor speeds are updated based on these inflow conditions, the mutual interference velocity, $v_{int,z}$, and the normal rotor force, P_x, are also updated, which requires an iterative approach to find the final thrust conditions of each rotor. A similar convergence approach can be applied to the force trim, RPM predictions due to mutual rotor wake interactions.

C. Drag Prediction of Standard Multirotor Vehicle Components

A typical multirotor vehicle is shown in Figure 4. Its performance can be predicted using a drag decomposition approach, that is, by adding the drag contributions of each of its elements. For example, the drag of the rotor arms, part C in Fig. 4, or legs, part D, can be approximated using drag values of cylinders. The fuselage, part E, can be approximated with the drag of a sphere, although previous wind-tunnel tests indicated that this particular configuration produces a downward force during flight and, subsequently, induced drag.[8] Similarly, the drag values of the payload, part F, and motor hubs, part B, can be approximated using standard shapes.

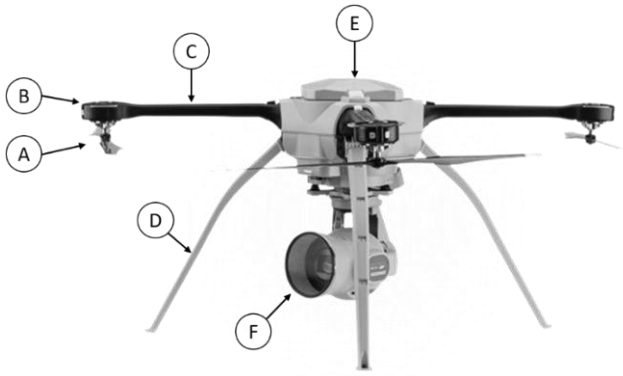

Figure 4: Standard multirotor components A) rotor, B) motor, C) rotor arm, D) landing gear (leg), E) central body, F) payload.[11]

As mentioned, the previous tests assessed the lift and drag behavior of this particular body, part E in Fig. 4. In this particular case, lift can be approximated well by assuming a circular wing.[8] The same tests indicated that drag can be estimated relatively accurately using the drag of a sphere plus the lift related drag of a circular wing. One should note, that under normal flight condition the vehicle has a pitch down orientation, which means that the lift produced by the body is downwards. This extra lift force can be as much as 10% of the vehicle weight.

III. Implementation

Figure 5 shows the implementation of force trim prediction and rotor interaction models used to determine the rotor power, rotor speeds and residual moments for force trimmed flight over a range of flight speeds. After developing the geometry and setting up the vehicle configuration, the algorithm loops over the flight speeds. Within the flight speed loop, after the required thrusts of each rotor is determined, an iteration is required to determine the conditions of each rotor after considering the interference velocities of the other rotors. Although his would require another iteration loop in order to account for the normal rotor force, P_x, its influence was found to be small and negligible for the trim solution. Once the mutual interference has led to a converged solution for all rotors, the power required for each rotor and the residual moments are calculated.

It takes about 1.5 minutes to compute the entire flight envelope of a typical multirotor vehicle like the one shown in Fig. 4 on a standard laptop with an Intel ® Core™ i7 processor. The interaction part typically converges in about 5 iterations. Preliminary comparisons with flight test data shows satisfactory agreement.[8] The computed data allows the examination of the performance of each rotor, as well the impact of other elements of the vehicle. In general, its computational speed makes it suitable for possible design studies.

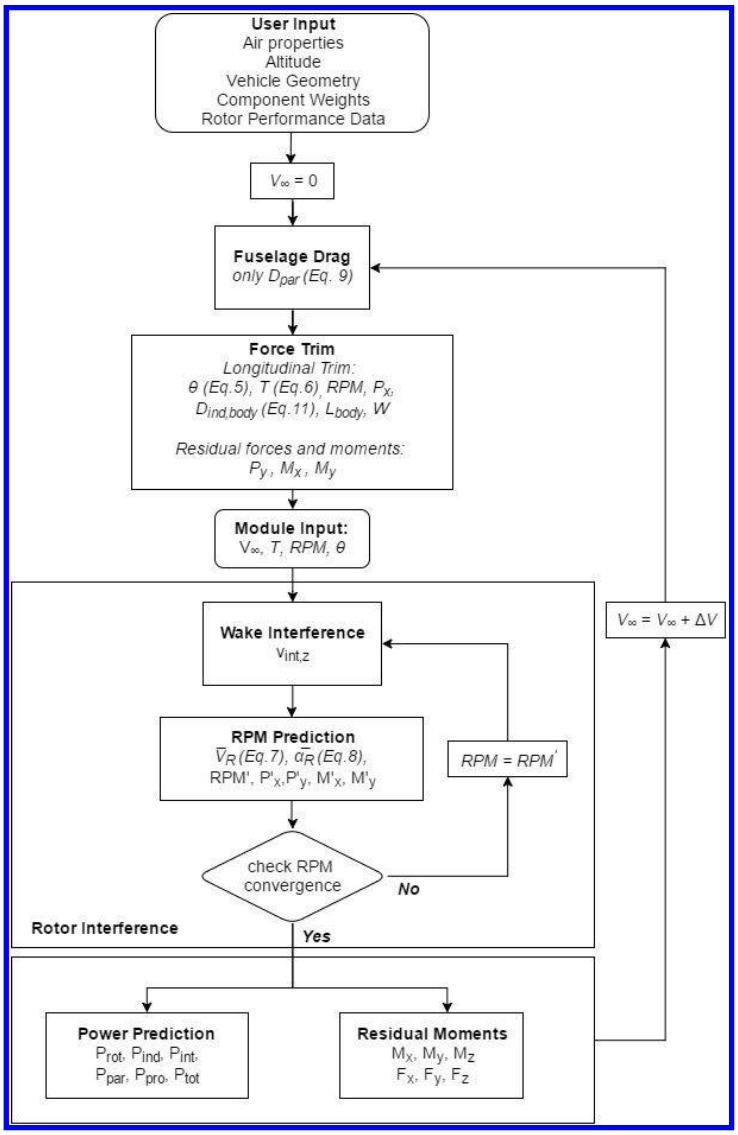

Figure 5: Implementation of multirotor vehicle performance model

IV. Performance Prediction Comparison Between Vehicle Orientations

Performance results were predicted using vehicle geometries of a four-rotor Aeryon SkyRanger and using T-Motor 18x6.1 rotor data that was developed using a blade element momentum theory approach.[9] The total vehicle mass was 3kg and flight conditions were set to standard seal-level conditions.

Rotor speed, rotor power, vehicle power, rotor interference velocities and residual moments were compared between two vehicle orientations: diamond and square. Diamond configuration refers to forward flight of a four-rotor vehicle with one leading rotor. Square configuration refers to forward flight with two leading rotors.

A. Rotor Interactions

Mutual interference velocities are predicted as the sum of velocities induced by rotor blades and rotor wakes modelled applied to a rotor of interest. Positive values indicate upwash velocities at a particular rotor due to the flow fields of the other rotors and negative velocities a downwash.

Figure 6 shows the rotor interference velocities of each rotor of the diamond and square configuration. In hover, each rotor causes equal upwash at the other rotors. Once the multirotor vehicle is in forward flight, the rear rotors experience an increased downwash and the lead rotors upwash. In the case of the two side rotors of the diamond configuration, the rotors see upwash benefits from the lead rotor and of each other. Furthermore, with growing flight speed, the lead rotor of the diamond configuration is increasingly exposed to the upwash of the downstream rotors. In the case of the square configuration, a growing increase in negative, downwash interference velocity is expected as the rear rotors are in the full wakes of the lead rotors.

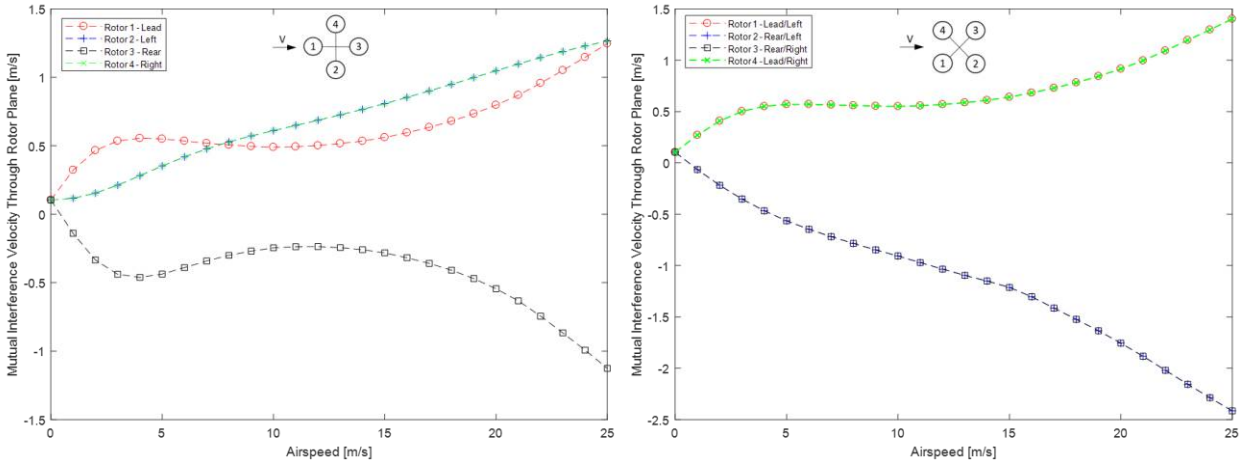

Figure 6: Mutual interference velocities applied to each rotor flying in diamond (left) and square (right) configurations

B. Rotor Speeds Required for Force Trim

Rotor speeds were obtained using the rotor interaction model. All four rotors had the same thrust requirement for force trimmed flight over a range of flight speeds between 0-25m/s. Figure 7 shows the effects of rotor interactions on rotor speeds compared to rotor speed predictions without applying the rotor interaction model. In the case of the diamond configuration, the two side rotors have the same results due to geometric symmetries about the x-axis of the vehicle. In square configuration, the two leading rotors equivalent results and the two rear equivalent results. Equivalent rotor speed results are displayed as overlapping trends on both graphs in Fig. 7.

The crossover point of lead and side rotor speed trends in diamond orientation around 8m/s coincides with the cross point of mutual interference velocities shown in Fig. 6. For either configuration, higher rotor speed requirements of the rear rotors are predicted due to the larger downwash that the trailing rotors experience in comparison to the lead rotors. The rear rotors need to work harder maintain the same thrust requirements at trim, whereas the lead rotors have the benefit of upwash contributions from the trailing rotors. Compared to the two rear rotors of the square formation, the rear rotor of the diamond configuration requires considerable lower rotational speeds, about 7.5% less at high speeds. In contrast, the lead rotors of each configuration have similar rotational speeds over most of the flight envelope. These differences in rotational speed requirements manifest themselves in power.

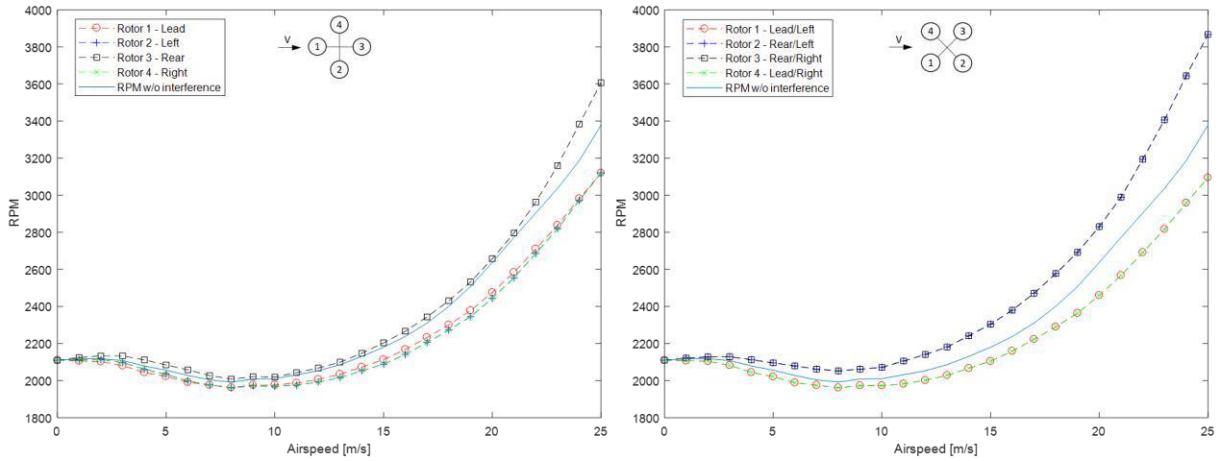

Figure 7: Rotor speeds required to maintain same thrust flying in diamond (left) and square (right) configurations

C. Power Prediction

Rotor power was predicted as the sum of rotor power as influenced by rotor power and parasitic power divided over the four rotors. The total power predictions of each rotor flying in diamond and square orientations is shown in Fig. 8. Relatively minimal changes in power requirements are seen at low flight speeds between all rotors in both flight configurations as the vehicle weight dominates the flight performance. Small power benefits are seen around 5m/s in both diamond and square orientation cases. The increase in rotor power requirements starting around 8m/s is reflective of the square of the flight speed and cube of the rotor rotational speed due to the parasitic power and rotor power contributions, respectively, at high flight speeds. Similar power trends are observed in helicopter performance.[12] The power increase of the rear rotors is generally larger than of the lead rotors. Similar to the rotational speed observations, the rear rotors of the square configuration have higher power needs compared to the rear rotor of the diamond configuration and the lead rotors seem to have similar power needs.

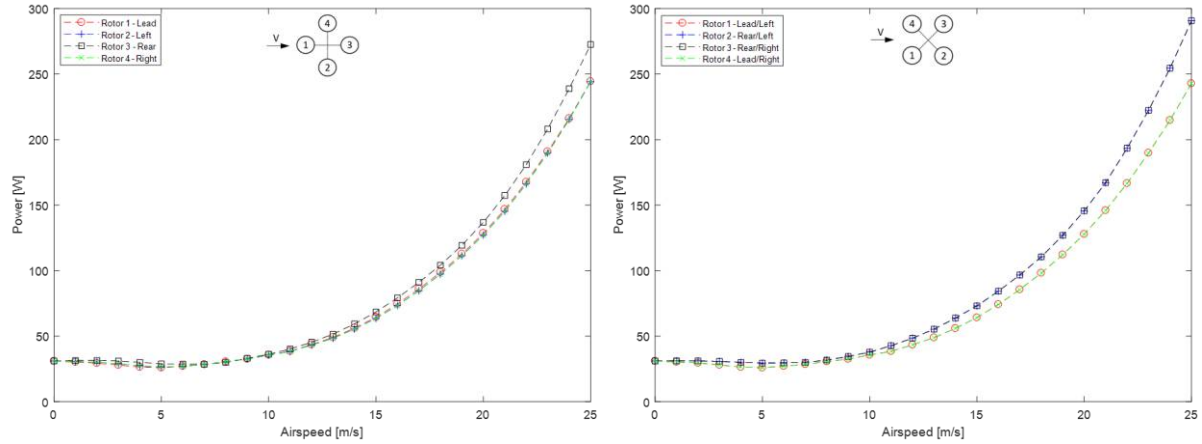

Figure 8: Total power of each rotor flying in diamond (left) and square (right) configurations

Figure 9 shows total vehicle power between diamond and square formations. Flying in diamond formation shows a power benefit of up to 6% at high speeds over square formation flight. This power benefit is attributed to the two rotors in square formation experiencing full downwash effects by the lead rotors as opposed to diamond formation where the one rear rotor will only see the full downwash effects of the one lead rotor and some of the downwash effects of the two side rotors. Another way to look at this is that, compared to the square configuration, the diamond configuration has a larger effective span with subsequent overall induced power benefits.

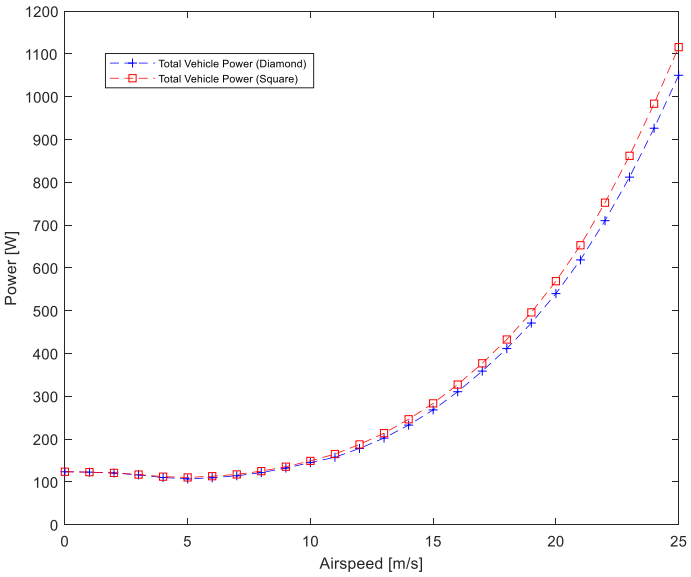

Figure 9: Total vehicle power between diamond and square configurations

D. Residual Moments in Longitudinal Force Trimmed Flight

Figure 10 shows residual pitching moments that result from the loads of the different components of the quadcopter show in in Fig. 4. The rotor performance is based on data predicted for a T-Motor 18x6.1 rotor. Residual moments were calculated with respect to the reference point at the center of the fuselage and based on rotor, drag and weight force and moment results. In general, the overall residual pitching moment increases with flight speed.

The most significant moment is caused by the positive pitching moments from the rotors. Rotor pitching moments are the result of increasingly nonuniform inflow conditions at the discs of the rotors with increasing forward speed. As a consequence of forward flight with significant edgewise flow component, the leading edge of the rotor discs experience less downwash, or even upwash, than the trailing edge of the rotor. These uneven inflow conditions result the positive pitching moments that dominate the vehicle.

Other major moment contributors, although with a pitch down effect, are due to the landing gear and payload, which have relatively high drags and are located below the reference point. Total in-plane rotor drag force, P_x, leads to a 6% higher positive overall pitching moment of the square configuration compared to the subsequent moment of the diamond configuration. The overall P_x moment contribution, however, is relatively minor compared to the other major pitching moment contributions of the rotor pitching moment, landing gear and payload.

Currently, by setting all rotor thrusts equal for force trim the total thrust moment in both configurations and at all flight speeds is zero. To achieve moment trim, the thrust components will need to produce a total negative pitching moment in order bring the current positive total vehicle pitching moment to zero. The rear rotors will require more thrust and the lead rotors less thrust to maintain force trim while bringing pitching moments to zero.

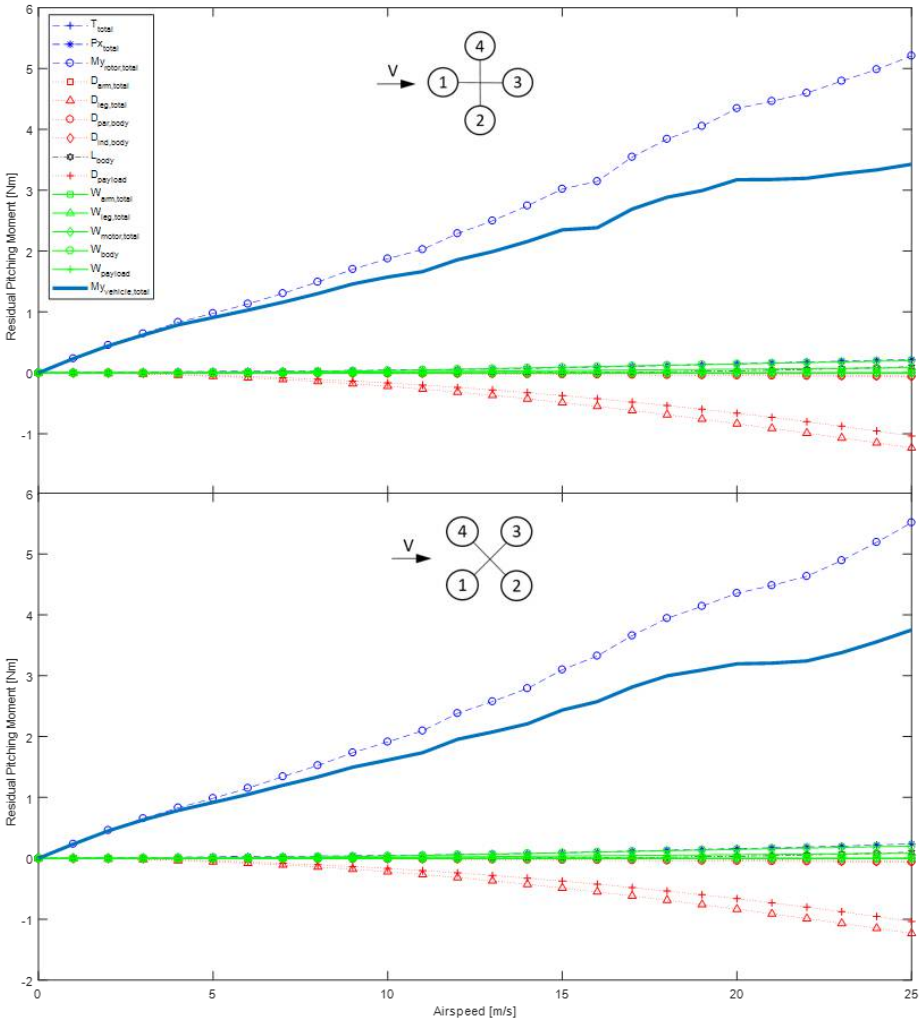

Figure 10: Residual moments generated at force trimmed conditions on a four-rotor SkyRanger vehicle using T-Motor 18x6.1 rotor

V. Conclusions

Rotor performance prediction improvements and residual moment calculations were incorporated into the multirotor vehicle performance prediction model. Using the rotor interaction model to predict rotor speeds provides a more comprehensive performance prediction method when determining power loss contributions of a multirotor vehicle design. Including residual moment predictions into the multirotor vehicle performance model gave insight into major force contributors that affect stability and control.

It was shown that the rear rotors in forward flight experience significant downwash effects caused by the mutual interference velocities of the lead rotors. The downwash effects resulted in greater rotors speeds and power requirements in order to maintain the force trim. Comparing the mutual interference velocities between each rotor over shows that the mutual rotor interference velocities are highly non-linear as vehicle pitch and thrust requirements increase in order to maintain force trim over a range of airspeeds. Velocity interactions applied to the rotors, however, still exclude any induced velocities due to the flow around the vehicle fuselage. Future work will include a body-flow interaction model that determines the induced velocities applied to the rotors using a potential flow method based on flow around a sphere representing the central body of the multirotor vehicle.

Acknowledgments

This research was made possible through a collaborative effort with Aeryon Labs Inc. and the WAVE Lab of the University of Waterloo that was made possible through funding by the Ontario Centres of Excellence.

References

[1]Khan, W., and Nahon, M., "Toward an accurate physics-based UAV thruster model," *IEEE/ASME Transactions on Mechatronics*, vol. 18, Aug. 2013, pp. 1269–1279.

[2]Theys, B., Dimitriadis, G., Hendrick, P., and De Schutter, J., "Experimental and Numerical Study of Micro-Aerial-Vehicle Propeller Performance in Oblique Flow," *Journal of Aircraft*, Oct. 2016, pp. 1–9.

[3]Carroll, T. B., George, I.-R., Bramesfeld, G., and Raahemifar, K., "Design Optimization of Small Rotors in Quad-Rotor Configuration," *54th AIAA Aerospace Sciences Meeting*, Jan. 2016, pp. 1–17.

[4]Luo, J., Zhu, L., and Yan, G., "Novel Quadrotor Forward-Flight Model Based on Wake Interference," *AIAA Journal*, vol. 53, Dec. 2015, pp. 3522–3533.

[5]Hoffmann, G. M., Huang, H., Waslander, S. L., and Tomlin, C. J., "Precision flight control for a multi-vehicle quadrotor helicopter testbed," *Control Engineering Practice*, vol. 19, Sept. 2011, pp. 1023–1036.

[6]Hoffmann, G. M., Waslander, S. L., and Tomlin, C. J., "Aerodynamics and Control of Autonomous Quadrotor Helicopters in Aggressive Maneuvering," *2009 IEEE International Conference on Robotics and Automation*, May 2009, pp. 1050-4729.

[7]Powers, C., Mellinger, D., Kushleyev, A., Kothmann, B., and Kumar, V., "Influence of Aerodynamics and Proximity Effects in Quadrotor Flight," *Springer Tracts in Advanced Robotics - Experimental Robotics*, vol. 88, 2013, pp. 289–302.

[8]George, I. E., "A Multirotor Vehicle Performance Prediction Method," Master's Thesis, Department of Aerospace Engineering, Ryerson University, 2017.

[9]Carroll, T. B., "A Design Methodology for Rotors of Small Multirotor Vehicles," Master's Thesis, Department of Aerospace Engineering, Ryerson University, 2017.

[10]Castles, W., and De Leeuw, J. H., "The Normal Component of the Induced Velocity in the Vicinity of a Lifting Rotor and Some Examples of its Application," *NACA Report 1184*, 1954.

[11]Aeryon Labs Inc, "Aeryon SkyRanger the benchmark for VTOL sUAS" Available: https://www.aeryon.com/aeryon-skyranger.

[12]Leishman, J. G., *Principles of Helicopter Aerodynamics*, New York, NY: Cambridge University Press, 2000.